

October 1, 2018

OCHA-PP-344

# Search for lepton flavor violation at future lepton colliders

Gi-Chol Cho<sup>a</sup>, Hanako Shimo<sup>b</sup>

<sup>a</sup>*Department of Physics, Ochanomizu University, Tokyo 112-8610, Japan*

<sup>b</sup>*Graduate school of Humanities and Sciences, Ochanomizu University, Tokyo 112-8610, Japan*

## Abstract

Lepton flavor violating (LFV) processes,  $e^+e^- \rightarrow e^+\ell^-$  and  $e^-e^- \rightarrow e^-\ell^-$  ( $\ell = \mu$  or  $\tau$ ), via four-Fermi contact interactions at future International Linear Collider (ILC) are studied. Taking account of previous experimental results of LFV processes  $\mu \rightarrow 3e$  and  $\tau \rightarrow 3e$ , we find that the upper limits on the LFV parameters for  $\ell = \tau$  could be improved at the ILC experiment using the polarized electron beam. The improvement of the upper limits could be nearly an order of magnitude as compared to previous ones.

arXiv:1612.07476v2 [hep-ph] 19 Jun 2017

# 1 Introduction

Discovery of the neutrino oscillation [1] implies the finite but tiny mass of neutrinos and opens a window to new physics beyond the Standard Model. One of the direct consequences of massive neutrinos is the lepton-flavor violating (LFV) processes, though the size of the signal is highly model dependent. For example, a simple extension of the SM which allows neutrinos to be massive predicts the branching ratio of  $\mu \rightarrow e\gamma$  as  $\text{Br}(\mu \rightarrow e\gamma) = \frac{3}{32\pi}\alpha|U_{ei}^*U_{\mu i}|^2(m_{\nu_i}/m_W)^4 < 10^{-48}(m_{\nu_i}/1 \text{ eV})^4$ , which is hopeless to be observed (where  $\alpha, U_{ij}$  and  $i$  denote the fine-structure constant, lepton-flavor mixing matrix and the generation index, respectively). In some class of new physics models, however, there could be sources of sizable LFV. Origin of the LFV and phenomenological predictions have been extensively studied based on various ideas such as supersymmetry [2, 3, 4, 5], extra-dimension [6, 7, 8], and so on [9].

Although no evidence of the LFV has been observed so far, several experiments are aiming to find signatures of LFV in the charged lepton sector, e.g.,  $\mu \rightarrow e\gamma$  at MEG II [10],  $\mu \rightarrow eee$  at Mu3e [11],  $\mu$ - $e$  conversion ( $\mu N \rightarrow eN$ ) at COMET [12] and Mu2e [13], the LFV in  $\tau$  decays at Belle II [14], etc (see e.g. [15, 16] for reviews). The sensitivities of (some of) these experiments to new physics search have been studied in, e.g., refs. [17, 18, 19], based on the effective Lagrangian with higher dimensional operators. In this paper, we investigate a possibility to search for the LFV processes from the four-Fermi contact interactions at the collider experiments. We focus the processes

$$e^+e^- \rightarrow e^+\ell^-, \tag{1}$$

$$e^-e^- \rightarrow e^-\ell^-, \tag{2}$$

for  $\ell = \mu, \tau$  at future  $e^+e^-$  linear collider (International Linear Collider, ILC) [20] and  $e^-e^-$  collider as its option<sup>1</sup>. The new physics effects on these processes can be parametrized by six couplings for each lepton flavor  $\ell$ , and we examine constraints on these parameters from the ILC experiments. We show that the ILC experiment is less sensitive than the previous LFV experiments for  $\ell = \mu$  case. On the other hand, upper bounds on the LFV parameters could be improved by more than an order of magnitude from the previous bound for  $\ell = \tau$  case, in particular by using the polarized electron beam. This paper is organized as follows. We briefly review the effective Lagrangian of four-Fermi contact interactions and some observables related to our study in Sec. II. Numerical analysis and limits on the LFV parameters will be given in Sec. III. Sec.IV is devoted to summary.

---

<sup>1</sup> A possibility of the LFV process (1) due to the sterile neutrino production and decay has been discussed in ref. [21], while the process (2) has been studied in the type-II seesaw model in ref. [22].

## 2 Four-fermi interactions and observables

The effective interaction Lagrangian describes the LFV processes via the four-Fermi contact interactions is given by [23]

$$\begin{aligned} \mathcal{L}_{\text{eff}} = & -\frac{4G_F}{\sqrt{2}} \{g_1^\ell (\bar{\ell}_R e_L) (\bar{e}_R e_L) + g_2^\ell (\bar{\ell}_L e_R) (\bar{e}_L e_R) \\ & + g_3^\ell (\bar{\ell}_R \gamma^\mu e_R) (\bar{e}_R \gamma_\mu e_R) + g_4^\ell (\bar{\ell}_L \gamma^\mu e_L) (\bar{e}_L \gamma_\mu e_L) \\ & + g_5^\ell (\bar{\ell}_R \gamma^\mu e_R) (\bar{e}_L \gamma_\mu e_L) + g_6^\ell (\bar{\ell}_L \gamma^\mu e_L) (\bar{e}_R \gamma_\mu e_R)\} + \text{h.c.}, \end{aligned} \quad (3)$$

where the Fierz rearrangement is used. The suffix  $\ell$  stands for  $\mu$  or  $\tau$ , and  $G_F$  denotes the Fermi coupling constant. The subscripts  $L$  and  $R$  represent the chirality of a fermion  $f$ , i.e.,  $f_{L(R)} \equiv \frac{1-(+)\gamma_5}{2} f$ . There are six dimensionless couplings  $g_i$  ( $i = 1 \sim 6$ ) but only three parameters are constrained from the LFV experiments as will be shown later.

In the limit of massless leptons, the spin-averaged differential cross-section in the center-of-mass (CM) system for  $e^+e^- \rightarrow e^+\ell^-$  and  $e^-e^- \rightarrow e^-\ell^-$  are calculated from the effective Lagrangian (3) as

$$\frac{d\sigma(e^+e^- \rightarrow e^+\ell^-)}{d\cos\theta} = \frac{G_F^2 s}{64\pi} [(G_{12}^\ell + 16G_{34}^\ell) (1 + \cos\theta)^2 + 4G_{56}^\ell \{4 + (1 - \cos\theta)^2\}], \quad (4)$$

$$\frac{d\sigma(e^-e^- \rightarrow e^-\ell^-)}{d\cos\theta} = \frac{G_F^2 s}{16\pi} [G_{12}^\ell + 16G_{34}^\ell + 2G_{56}^\ell (1 + \cos\theta)^2], \quad (5)$$

where  $\sqrt{s}$  denotes the total energy in the CM-system and the parameter  $G_{ij}^\ell$  is defined as

$$G_{ij}^\ell \equiv |g_i^\ell|^2 + |g_j^\ell|^2. \quad (6)$$

The couplings in the effective Lagrangian (3) also induce the LFV process  $\mu \rightarrow eee$  or  $\tau \rightarrow eee$  (hereafter we denote these processes as  $\mu \rightarrow 3e$  and  $\tau \rightarrow 3e$  for simplicity). The branching ratio of  $\mu \rightarrow 3e$  is expressed in terms of  $G_{ij}^\mu$  as [24]

$$\text{Br}(\mu \rightarrow 3e) = \frac{\Gamma(\mu \rightarrow 3e)}{\Gamma(\mu \rightarrow e\nu_\mu\bar{\nu}_e)} = \frac{1}{8} (G_{12}^\mu + 16G_{34}^\mu + 8G_{56}^\mu), \quad (7)$$

while that of  $\tau \rightarrow 3e$  is

$$\begin{aligned} \text{Br}(\tau \rightarrow 3e) &= \frac{\tau_\tau}{\tau_\mu} \left(\frac{m_\tau}{m_\mu}\right)^5 \times \frac{1}{8} (G_{12}^\tau + 16G_{34}^\tau + 8G_{56}^\tau) \\ &\approx 0.022 \times (G_{12}^\tau + 16G_{34}^\tau + 8G_{56}^\tau), \end{aligned} \quad (8)$$

where  $\tau_\tau$  and  $\tau_\mu$  are the lifetime of  $\tau$  and  $\mu$ , respectively, and we adopt  $\tau_\tau = 2.91 \times 10^{-13}$  s and  $\tau_\mu = 2.20 \times 10^{-6}$  s for the numerical evaluation [25]. To find constraints on the LFV parameter  $G_{ij}$  from  $\mu \rightarrow 3e$  and  $\tau \rightarrow 3e$ , we summarize current experimental bounds on

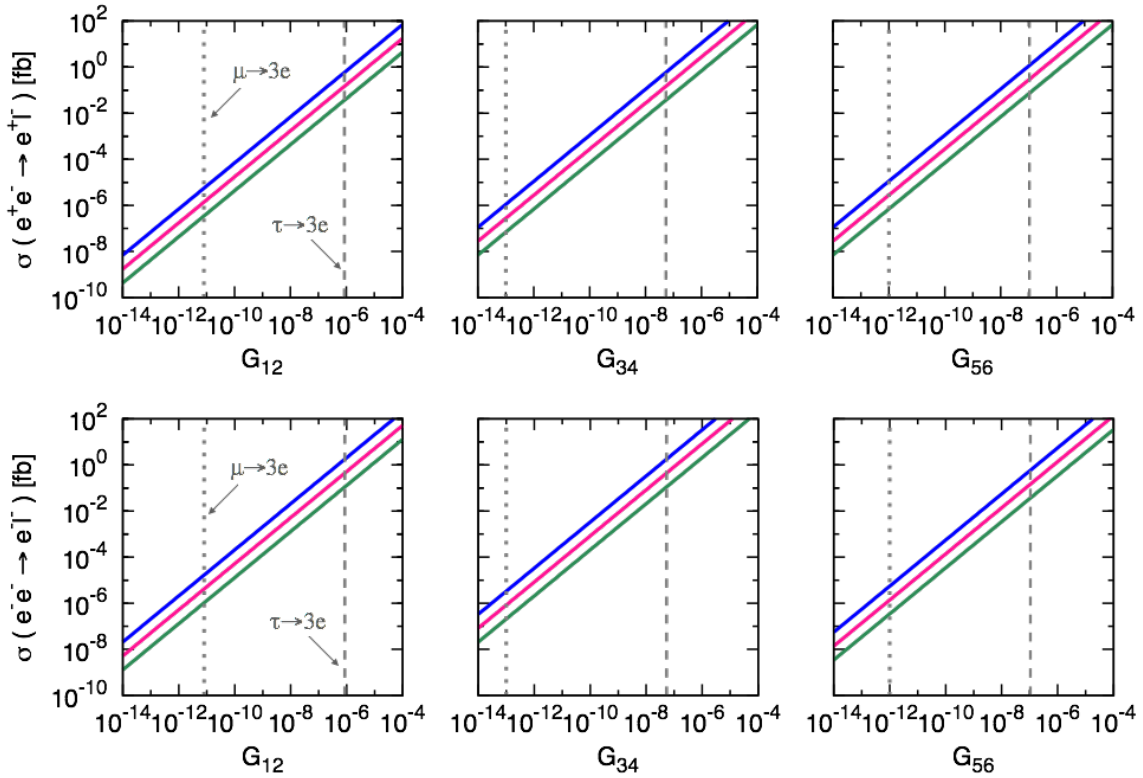


Figure 1: The cross section of  $e^+e^- \rightarrow e^+\ell^-$  (upper) and  $e^-e^- \rightarrow e^-\ell^-$  (lower) for  $\sqrt{s} = 250$  GeV (green), 500 GeV (red) and 1 TeV (blue). The dotted and dashed vertical lines denote the upper bounds on  $G_{ij}$  from  $\mu \rightarrow 3e$  [26] and  $\tau \rightarrow 3e$  [27].

those processes. The upper bounds on  $\text{Br}(\mu^+ \rightarrow e^+e^+e^-)$  and  $\text{Br}(\tau \rightarrow 3\ell)$  have been given by the SINDRUM [26] and the Belle [27] collaborations, respectively:

$$\text{Br}(\mu^+ \rightarrow e^+e^+e^-) < 1.0 \times 10^{-12}, \quad (9)$$

$$\text{Br}(\tau^- \rightarrow e^-e^+e^-) < 2.7 \times 10^{-8}. \quad (10)$$

The experimental limits (9) and (10) can be read as constraints on the LFV parameter  $G_{ij}$  through eqs. (7) and (8).

In Fig. 1, we show the cross sections for  $e^+e^- \rightarrow e^+\ell^-$  (upper) and  $e^-e^- \rightarrow e^-\ell^-$  (lower) from eqs. (4) and (5) with the pseudo-rapidity  $|\eta| \leq 2.5$  as functions of the LFV parameter  $G_{12}$  (left),  $G_{34}$  (center) and  $G_{56}$  (right). In each figure, the cross section is evaluated varying only  $G_{ij}$  shown at the horizontal axis, and the other two parameters are set to be zero. The green, red and blue lines correspond to the CM energy  $\sqrt{s} = 250$  GeV, 500 GeV and 1 TeV, respectively. The dotted and dashed vertical lines denote constraints on  $G_{ij}$  from SINDRUM for  $\ell = \mu$  and Belle for  $\ell = \tau$ , respectively.

It can be seen from Fig. 1 that the LFV parameter  $G_{ij}$  for  $\ell = \mu$  is strongly constrained from  $\mu \rightarrow 3e$ . Taking account of the bounds on  $G_{ij}$  for  $\ell = \mu$ , the cross sections are roughly

smaller than  $10^{-5}$  fb for both  $e^+e^- \rightarrow e^+\mu^-$  and  $e^-e^- \rightarrow e^-\mu^-$ , which are too small to observe the LFV process at the ILC. On the other hand, since current limits on  $G_{ij}$  for  $\ell = \tau$  are much weaker than the  $\mu$ -channel, it could be expected that the ILC experiment has a certain sensitivity for exploring the LFV processes using the  $\tau$ -channel. We, therefore, focus on the  $\ell = \tau$  case in the following study<sup>2</sup>. It should be noted that the limit of the LFV decay  $\tau \rightarrow 3\ell$  is expected to be improved significantly in the level of  $O(10^{-10})$  at the super-KEKB [28].

### 3 Constraints on the LFV parameters at the ILC

Next we study constraints on the LFV parameter  $G_{ij}$  expected at the ILC experiments. The SM background processes on the signal processes (1) and (2) are

$$e^+e^- \rightarrow e^+\nu_e\tau^-\bar{\nu}_\tau, \quad (11)$$

$$e^-e^- \rightarrow e^-\nu_e\tau^-\bar{\nu}_\tau. \quad (12)$$

To estimate the background events quantitatively, we generate these processes using MADGRAPH5\_AMC@NLO [29] with the pseudo rapidity  $|\eta| \leq 2.5$ . We summarize the cross section of the SM background processes (11) and (12) for  $\sqrt{s} = 250$  GeV, 500 GeV and 1 TeV in Table 1. Then the upper limits of the LFV parameters are examined using the

	$\sqrt{s} = 250$ GeV	500 GeV	1 TeV
$\sigma(e^+e^- \rightarrow e^+\nu_e\tau^-\bar{\nu}_\tau)$ [fb]	203	113	85.5
$\sigma(e^-e^- \rightarrow e^-\nu_e\tau^-\bar{\nu}_\tau)$ [fb]	29.7	122	198

Table 1: Summary of cross section of the background processes (11) and (12) for  $\sqrt{s} = 250$  GeV, 500 GeV and 1 TeV obtained by MADGRAPH5\_AMC@NLO [29].

$\chi^2$ -function defined as

$$\chi^2 \equiv \frac{(N_{S+B} - N_B)^2}{N_B}, \quad (13)$$

where subscripts S and B denote the signal and background respectively. The number of event  $N$  is defined from the cross section  $\sigma$  and the integrated luminosity  $\int dt\mathcal{L}$  as  $N \equiv \sigma \cdot \int dt\mathcal{L}$ . In the following analysis, we use the set of  $\sqrt{s}$  and the luminosity at each phase of the ILC experiment [30] as summarized in Table 2. We set the 95% CL limit on the LFV parameters at  $\chi^2 = 3.84$ .

We show  $\chi^2$  as a function of the LFV parameter for  $e^+e^- \rightarrow e^+\tau^-$  (upper) and  $e^-e^- \rightarrow e^-\tau^-$  (lower) in Fig. 2. The green, red and blue curves are obtained using (i), (ii) and (iii)

<sup>2</sup>hereafter we suppress the index  $\ell$  in  $G_{ij}^\ell$ .

	(i)	(ii)	(iii)
$\sqrt{s}$ (GeV)	250	500	1000
$\mathcal{L}$ ( $10^{34}$ cm $^{-2}$ s $^{-1}$ )	0.75	3.6	3.6

Table 2: summary of center-of-mass energy ( $\sqrt{s}$ ) and luminosity planned at the ILC experiment [30].

in Table 2, respectively. The vertical dashed-line in each figure denotes the upper bound on  $G_{ij}$  from  $\text{Br}(\tau \rightarrow 3e)$ ;

$$G_{12} < 9.0 \times 10^{-7}, \quad G_{34} < 5.6 \times 10^{-8}, \quad G_{56} < 1.1 \times 10^{-7}. \quad (14)$$

The horizontal-dashed line represents  $\chi^2 = 3.84$ . We find that, for both  $\sqrt{s} = 250$  GeV (i) and 500 GeV (ii), none of three LFV parameters are improved over the upper limits from  $\text{Br}(\tau \rightarrow 3e)$  (14). For  $\sqrt{s} = 1$  TeV, the upper limits at 95% CL on  $G_{56}$  in the  $e^+e^-$  collision and  $G_{12}, G_{34}$  in the  $e^-e^-$  collision are better than those from  $\text{Br}(\tau \rightarrow 3e)$  (14), but the improvement is marginal.

Next we discuss a possibility to use the polarized electron beam. In many of the Feynman diagrams for the background processes (11) and (12), the initial electron couples to the  $W$ -boson which appears in the intermediate state. Contributions from such diagrams are suppressed when the electron beam is polarized to be right-handed, since only the left-handed electron can couple to the  $W$ -boson. In Fig. 3, we show  $\chi^2$  as a function of  $G_{ij}$  for

	$\sqrt{s} = 250$ GeV	500 GeV	1 TeV
$\sigma(e^+e_R^- \rightarrow e^+\nu_e\tau^-\bar{\nu}_\tau)$ [fb]	3.45	0.827	0.256
$\sigma(e^-e_R^- \rightarrow e^-\nu_e\tau^-\bar{\nu}_\tau)$ [fb]	6.95	15.0	12.4

Table 3: Summary of cross section of the background processes (11) and (12) for  $\sqrt{s} = 250$  GeV, 500 GeV and 1 TeV obtained by MADGRAPH5\_AMC@NLO [29].

the  $e^+e_R^-$  (upper) and the  $e^-e_R^-$  (lower) collisions. As we expected, the suppression of the SM background processes due to the right-handed electron beam makes the upper limits on the LFV parameter  $G_{ij}$  better than the unpolarized case shown in Fig. 2. For the  $e^+e_R^-$  collision, the 95% CL upper limits on three LFV parameters for  $\sqrt{s} = 1$  TeV are

$$G_{12} < 1.8 \times 10^{-7}, \quad G_{34} < 1.0 \times 10^{-8}, \quad G_{56} < 1.1 \times 10^{-8}, \quad (15)$$

which are a few factors smaller than those from  $\text{Br}(\tau \rightarrow 3e)$  at the Belle experiment (14). On the other hand, the bounds on  $G_{ij}$  for both  $\sqrt{s} = 250$  GeV and 500 GeV are still worse than those in  $\tau \rightarrow 3e$ , except for  $G_{56}$  for  $\sqrt{s} = 500$  GeV which is comparable with  $\text{Br}(\tau \rightarrow 3e)$ .

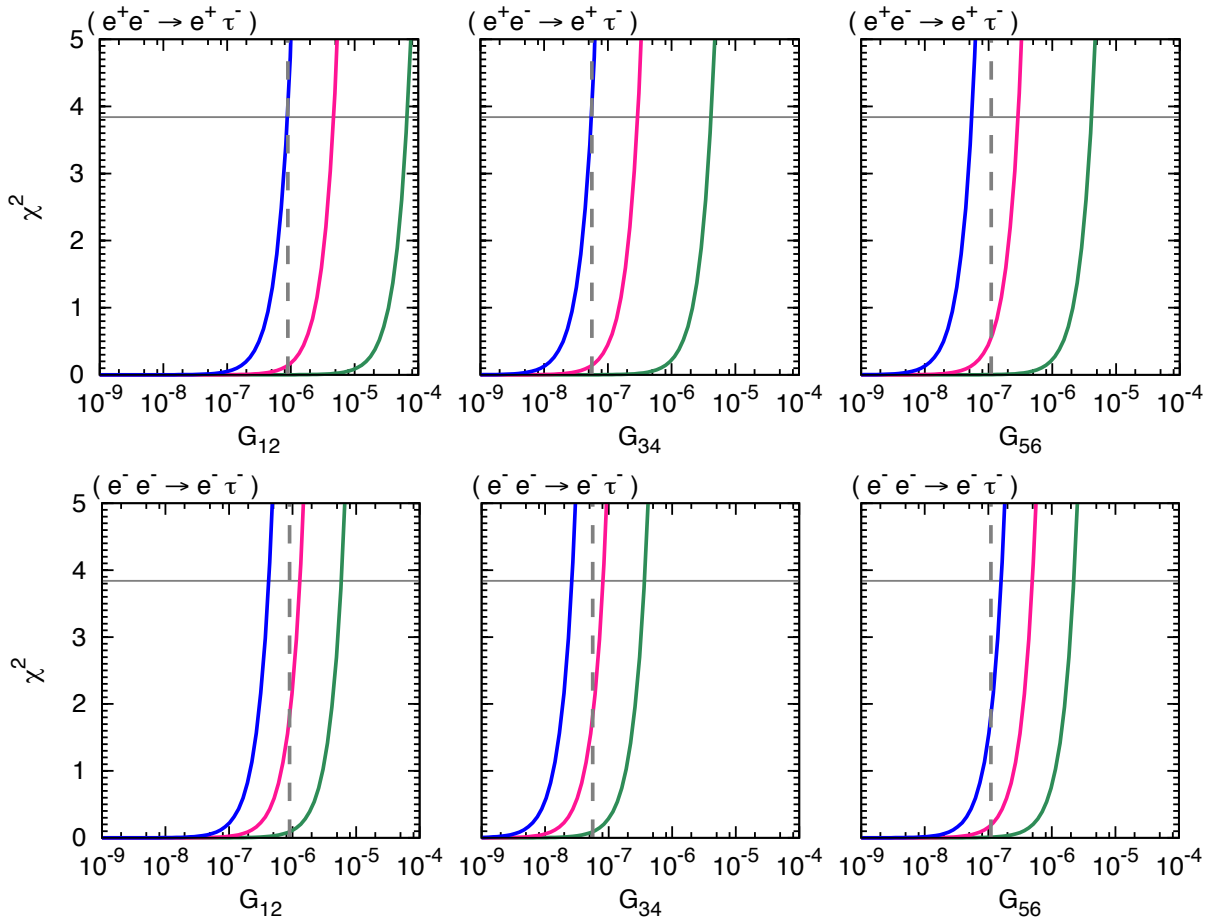


Figure 2: The  $\chi^2$ -parameters as functions of  $G_{12}, G_{34}$  and  $G_{56}$  for  $e^+e^-$  (upper) and  $e^-e^-$  (lower) collisions. The parameters (i), (ii) and (iii) in Table 2 are used to obtain green, red and blue curves, respectively. The vertical line denotes the upper bound on  $G_{ij}$  from  $\tau \rightarrow 3e$  and the horizontal-dashed line represents  $\chi^2 = 3.84$ .

In the  $e^-e^-_R$  collision, the upper limits on  $G_{ij}$  are improved further. For  $\sqrt{s} = 500$  GeV, the upper limits at 95% CL are given as

$$G_{12} < 2.2 \times 10^{-7}, \quad G_{34} < 1.3 \times 10^{-8}, \quad G_{56} < 8.5 \times 10^{-8}, \quad (16)$$

and those for  $\sqrt{s} = 1$  TeV are given as

$$G_{12} < 5.0 \times 10^{-8}, \quad G_{34} < 3.1 \times 10^{-9}, \quad G_{56} < 1.9 \times 10^{-8}, \quad (17)$$

which are better than the limits from  $\text{Br}(\tau \rightarrow 3e)$  (14).

We have so far discussed the search limits on the LFV processes at the ILC without taking account of the decay of the  $\tau$ -lepton in the final states. The ILC is expected to achieve a good detector performance for efficiency and purity of the main  $\tau$ -decay mode selections [31], as shown in Table 4 together with the experimental data of branching ratio [25]. The efficiency and purity in the table were calculated from  $\tau^+\tau^-$  production events, in which two

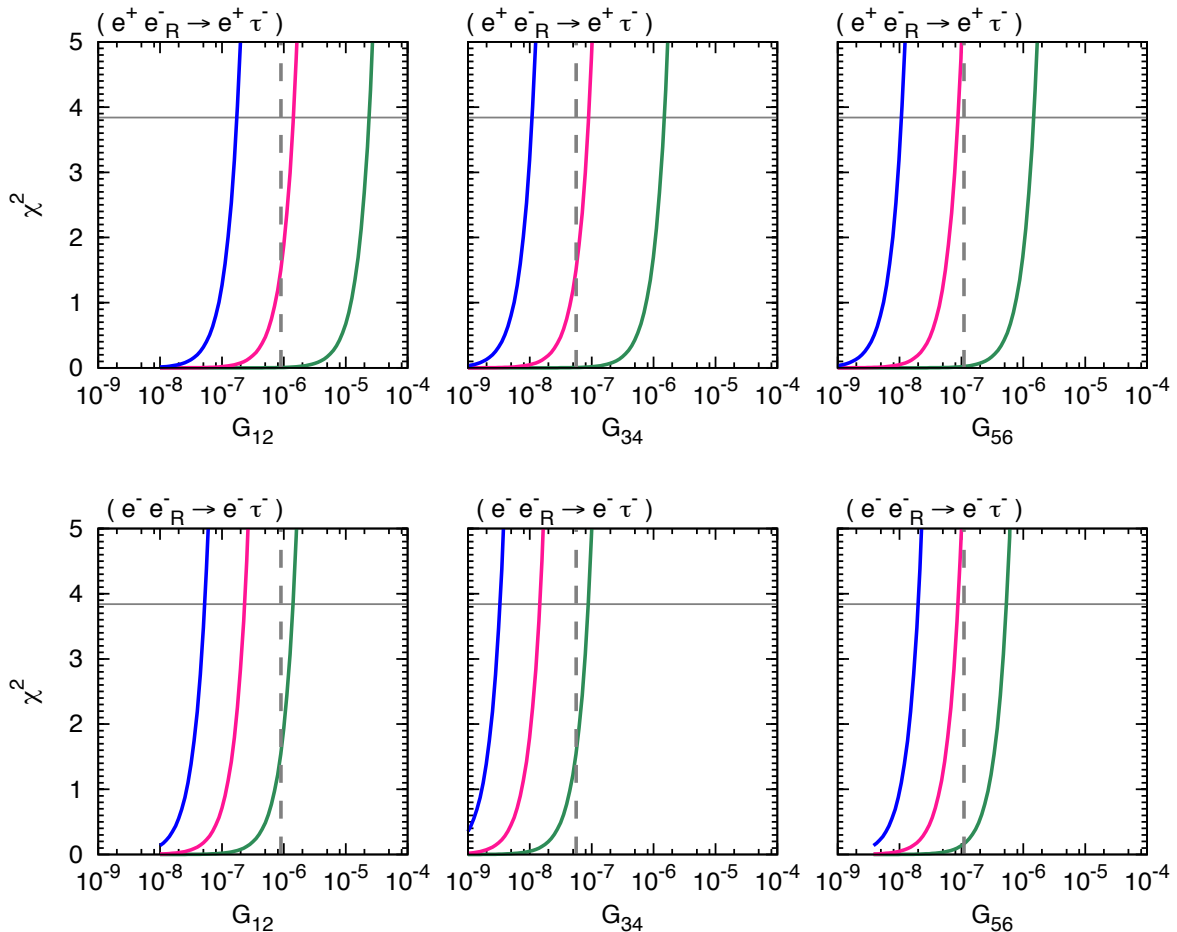


Figure 3: The  $\chi^2$ -parameters as functions of  $G_{12}$ ,  $G_{34}$  and  $G_{56}$  for  $e^+e^-$  (upper) and  $e^-e^-$  (lower) collisions.

$\tau$  candidates are required to be almost back-to-back. It is, therefore, a good approximation to assume 100% efficiency of these decay modes in the following discussion. Using three decay modes in Table 4, we find that the upper bounds of the LFV parameter are twice  $(1/(0.178+0.174+0.108)=2.17)$  as large as (15), (16) and (17). For example, the upper limits at 95% CL for  $\sqrt{s} = 1$  TeV in the  $e^-e^-$  collision are given as

$$G_{12} < 1.1 \times 10^{-7}, \quad G_{34} < 6.8 \times 10^{-9}, \quad G_{56} < 4.2 \times 10^{-8}. \quad (18)$$

The improvement is nearly an order of magnitude in  $G_{12}$  and  $G_{34}$ .

## 4 Summary

In summary, we have investigated constraints on four-Fermi contact interactions which leads to the LFV processes at the ILC experiments. The cross sections for both  $e^+e^- \rightarrow e^+\ell^-$  and  $e^-e^- \rightarrow e^-\ell^-$  are parametrized by three LFV parameters,  $G_{12}^\ell$ ,  $G_{34}^\ell$  and  $G_{56}^\ell$ , for each



Mode	Branching ratio [25]	Efficiency [31]	Purity [31]
$e^- \bar{\nu}_e \nu_\tau$	17.8%	98.9%	98.9%
$\mu^- \bar{\nu}_\mu \nu_\tau$	17.4%	98.8%	99.3%
$\pi^- \nu_\tau$	10.8%	96.0%	89.5%

Table 4: Branching ratio, efficiency and purity of main  $\tau$  decay modes.

lepton flavor  $\ell$ . Taking account of constraints from measurements of  $\text{Br}(\mu \rightarrow 3e)$  at the SINDRUM experiment and  $\text{Br}(\tau \rightarrow 3e)$  at the Belle experiment, we studied the upper limit on  $G_{ij}$  expected at the ILC experiments. Although the ILC cannot give better bounds on the LFV parameters than those at the SINDRUM experiment for  $\ell = \mu$ , we found that the measurements of cross sections of  $e^+e^- \rightarrow e^+\tau^-$  and  $e^-e^- \rightarrow e^+\tau^-$  at the ILC experiment could improve the upper limits on the LFV parameters over those at the Belle experiment. In particular, the use of polarized electron beam increases the sensitivity of measurements of the signal events by suppressing the SM background significantly. Owing to the expected high-efficiency of main  $\tau$  decay modes at the ILC, we found that the 95% CL upper limits on the LFV parameters at the ILC are in the level of  $O(10^{-7} - 10^{-9})$  for  $\sqrt{s} = 1$  TeV, which are better than the previous experiment nearly an order of magnitude.

## Acknowledgments

The work of G.C.C is supported in part by Grants-in-Aid for Scientific Research from the Japan Society for the Promotion of Science (No.16K05314).

## References

- [1] Y. Fukuda *et al.* [Super-Kamiokande Collaboration], Phys. Rev. Lett. **81**, 1562 (1998) [hep-ex/9807003].
- [2] R. Barbieri and L. J. Hall, Phys. Lett. B **338**, 212 (1994) [hep-ph/9408406].
- [3] R. Barbieri, L. J. Hall and A. Strumia, Nucl. Phys. B **445**, 219 (1995) [hep-ph/9501334].
- [4] J. Hisano, T. Moroi, K. Tobe, M. Yamaguchi and T. Yanagida, Phys. Lett. B **357**, 579 (1995) [hep-ph/9501407].
- [5] J. Hisano, T. Moroi, K. Tobe and M. Yamaguchi, Phys. Rev. D **53**, 2442 (1996) [hep-ph/9510309].
- [6] W. F. Chang and J. N. Ng, Phys. Rev. D **71**, 053003 (2005) [hep-ph/0501161].

- [7] K. Agashe, A. E. Blechman and F. Petriello, *Phys. Rev. D* **74**, 053011 (2006) [hep-ph/0606021].
- [8] C. Csaki, C. Delaunay, C. Grojean and Y. Grossman, *JHEP* **0810**, 055 (2008) [arXiv:0806.0356 [hep-ph]].
- [9] A. de Gouvea and P. Vogel, *Prog. Part. Nucl. Phys.* **71**, 75 (2013) [arXiv:1303.4097 [hep-ph]].
- [10] A. M. Baldini *et al.*, “MEG Upgrade Proposal,” arXiv:1301.7225 [physics.ins-det].
- [11] A. Bravar [Mu3e Collaboration], *Nucl. Part. Phys. Proc.* **260**, 155 (2015).
- [12] Y. Kuno [COMET Collaboration], “A search for muon-to-electron conversion at J-PARC: The COMET experiment,” *PTEP* **2013**, 022C01 (2013).
- [13] L. Bartoszek *et al.* [Mu2e Collaboration], “Mu2e Technical Design Report,” arXiv:1501.05241 [physics.ins-det].
- [14] T. Aushev *et al.*, arXiv:1002.5012 [hep-ex].
- [15] W. J. Marciano, T. Mori and J. M. Roney, *Ann. Rev. Nucl. Part. Sci.* **58**, 315 (2008).
- [16] R. H. Bernstein and P. S. Cooper, *Phys. Rept.* **532**, 27 (2013) [arXiv:1307.5787 [hep-ex]].
- [17] M. Koike, Y. Kuno, J. Sato and M. Yamanaka, *Phys. Rev. Lett.* **105**, 121601 (2010) [arXiv:1003.1578 [hep-ph]].
- [18] Y. Uesaka, Y. Kuno, J. Sato, T. Sato and M. Yamanaka, arXiv:1603.01522 [hep-ph].
- [19] A. Crivellin, S. Najjari and J. Rosiek, *JHEP* **1404**, 167 (2014) [arXiv:1312.0634 [hep-ph]].
- [20] H. Baer *et al.*, “The International Linear Collider Technical Design Report - Volume 2: Physics,” arXiv:1306.6352 [hep-ph].
- [21] S. Antusch, E. Cazzato and O. Fischer, arXiv:1612.02728 [hep-ph].
- [22] W. Rodejohann and H. Zhang, *Phys. Rev. D* **83**, 073005 (2011) [arXiv:1011.3606 [hep-ph]].
- [23] Y. Kuno and Y. Okada, *Rev. Mod. Phys.* **73**, 151 (2001) [hep-ph/9909265].
- [24] Y. Okada, K. i. Okumura and Y. Shimizu, *Phys. Rev. D* **61**, 094001 (2000) [hep-ph/9906446].

- [25] K. A. Olive *et al.* [Particle Data Group Collaboration], *Chin. Phys. C* **38**, 090001 (2014).
- [26] U. Bellgardt *et al.* [SINDRUM Collaboration], *Nucl. Phys. B* **299**, 1 (1988).
- [27] K. Hayasaka *et al.*, *Phys. Lett. B* **687**, 139 (2010) [arXiv:1001.3221 [hep-ex]].
- [28] A. J. Bevan *et al.* [BaBar and Belle Collaborations], *Eur. Phys. J. C* **74**, 3026 (2014) [arXiv:1406.6311 [hep-ex]].
- [29] J. Alwall *et al.*, *JHEP* **1407**, 079 (2014) [arXiv:1405.0301 [hep-ph]].
- [30] T. Behnke *et al.*, arXiv:1306.6327 [physics.acc-ph].
- [31] T. Behnke *et al.*, arXiv:1306.6329 [physics.ins-det].